JCTC Journal of Chemical Theory and Computation

Article

pubs.acs.org/JCTC

*GW*100: A Plane Wave Perspective for Small Molecules

Emanuele Maggio,[†] Peitao Liu,[†,‡] Michiel J. van Setten,[¶] and Georg Kresse*[,†]

[†]Faculty of Physics and Center for Computational Materials Science, University of Vienna, Sensengasse 8/12, A-1090 Vienna, Austria

[‡]Institute of Metal Research, Chinese Academy of Sciences, Shenyang 110016, China

[¶]Nanoscopic Physics, Institute of Condensed Matter and Nanosciences, Université Catholique de Louvain, 1348 Louvain-la-Neuve, Belgium

ABSTRACT: In a recent work, van Setten and co-workers have presented a carefully converged G_0W_0 study of 100 closed shell molecules [*J. Chem. Theory Comput.* **2015**, *11*, 5665−5687]. For two different codes they found excellent agreement to within a few 10 meV if identical Gaussian basis sets were used. We inspect the same set of molecules using the projector augmented wave method and the Vienna ab initio simulation package (VASP). For the ionization potential, the basis set extrapolated plane wave results agree very well with the Gaussian basis sets, often reaching better than 50 meV agreement. In order to achieve this agreement, we correct for finite basis set errors as well as errors introduced by periodically repeated images. For positive electron affinities differences between Gaussian basis sets and VASP are slightly larger. We attribute this to larger basis set extrapolation errors for the Gaussian basis sets. For quasi particle (QP) resonances above the vacuum level, differences between VASP and Gaussian basis sets are, however, found to be substantial. This is tentatively explained by insufficient basis set convergence of the Gaussian type orbital calculations as exemplified for selected test cases.

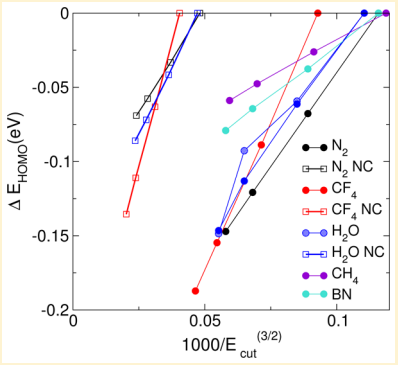

1. INTRODUCTION

The *GW* approximation suggested by Lars Hedin[1] has a long history in solid state physics. First practical applications already published in the 1980s by Hanke and co-workers were soon followed by the often quoted study of Hybertsen and Louie.[2−5] For solids, it is generally found that even the simplest approximation G_0W_0 yields reasonably accurate quasiparticle (QP) energies and band gaps in good agreement with experiment.[6−8] The results often improve if the Green's function is iterated to self-consistency, either updating the QP-energies only or even the one-electron orbitals.[6,7,9−15] Applications of the *GW* approximation to molecules, however, have been comparatively rare, since codes based on local orbitals, which are by construction particularly well suited to treat molecules, did not incorporate the *GW* approximation until recently. This has changed, with many local basis set codes, such as FHI-aims, MOLGW, Turbomole, and CP2K now supporting *GW* calculations.[16−22] Also, efficient plane wave codes using a Sternheimer approach, such as ABINIT and West,[23,24] are becoming available. As for solids, carefully converged QP calculations are, however, still comparatively scarce.[25]

To fill this gap, Bruneval recently performed systematic studies for about 30 molecules.[26] van Setten and co-workers went one step further and evaluated basis set extrapolated *GW* QP energies for 100 closed shell molecules using several codes.[27] They found that the *GW* QP energies of the highest occupied orbital (HOMO) and lowest unoccupied orbital (LUMO) of two local basis set codes, FHI-aims and Turbomole, virtually agree, *if identical basis sets are used*. In many respects this is not astonishing, since two codes ought to yield the same results, if the computational parameters are identical. The two codes are, however, technically quite different. For instance, they introduce auxiliary basis sets to avoid storing the two-electron four orbital integrals. Furthermore, FHI-aims uses a numerical representation of the Gaussians and calculates the self-energy along the imaginary axis (Wick rotation) requiring an analytic continuation to the real axis. All these factors can introduce small uncertainties. Clearly, the study impressively demonstrates that all these intricacies are well under control, and technically well converged results can be obtained using both codes.

The paper by van Setten et al.[27] also reports results using the *GW* Berkeley plane wave code.[28] Although agreement of that code with experiment is very good if the plasmon-pole model is used, comparison of the fully frequency dependent G_0W_0 HOMO and LUMO with Gaussian basis set results is less satisfactory. For the considered molecules, the mean absolute difference between Gaussian type orbitals (GTO) and plane waves (PWs) is about 200 meV for the HOMO. We note on passing that the agreement between GTO and other plane wave studies is seemingly superior,[23,24] although, this could be related to the fact that these studies only considered a subset of the *GW*100 set. The disagreement between the Berkeley *GW* PW code and GTO codes is certainly slightly disconcerting, since it puts decades of studies using PW based *GW* calculations into question. Remarkably, on the level of DFT,

Received: November 24, 2016
Published: January 17, 2017

DOI: 10.1021/acs.jctc.6b01150
J. Chem. Theory Comput. 2017, 13, 635−648

the reported one-electron energies of the HOMO agree to within a few 10 meV. So how can one understand the much larger discrepancies for *GW* QP energies?

A partial answer is given by the observation that QP energies converge very slowly with respect to the basis set size, as well established for Gaussian type orbitals.[20,26,27] van Setten et al. obtained basis set converged QP energies by extrapolating against the basis set size or against $1/C_n^3$, where C_n is the basis set cardinal number.[27] Extrapolation was based on def2-SVP, def2-TZVP, and def2-QZVP, but even though def2-QZVP constitutes a fairly complete set, the extrapolated values can differ by more than 300 meV from the values at the largest considered basis set. Astonishingly, the reported PW results were not extrapolated to the basis set limit, although a recent work of Klimes et al. shows that the *GW* QP energies converge like one over the number of plane waves,[25] and this behavior is also confirmed by purely analytical arguments.[29] Early evidence of this slow convergence using PWs exist aplenty.[30−32] In view of this slow convergence, a brute force approach to predict QP energies seems elusive considering that most codes scale cubically with respect to the number of basis functions. The present work tries to rectify this issue by reporting QP energies using the plane wave code VASP, carefully correcting for basis set incompleteness errors, as detailed in section 2.

Another point that we briefly mention in section 3 is that the calculation of the poles of the G_0W_0 Green's function can be unphysical, if the initial Green's function yields too small excitation energies. In this case, first linearizing the G_0W_0 self-energy and then determining the poles of the Green's function yields more robust QP energies. We, finally, finish with discussions and our conclusions.

2. THEORY AND COMPUTATIONAL METHOD

2.1. Theory. *GW* is a well established perturbative approach to calculate QP energies.[1] In the *GW* approximation, one initiates the calculations using a groundstate DFT calculation to obtain the DFT one-electron orbitals ϕ_n and the corresponding one-electron energies ϵ_n.

The first step in a *GW* calculation is to determine the DFT Green's functions

$$G_0(\mathbf{r}', \mathbf{r}, \omega) = \sum_n \frac{\phi_n(\mathbf{r}')\phi_n^*(\mathbf{r})}{\omega - \epsilon_n - i\eta\mathrm{sign}(\mu - \epsilon_n)} \tag{1}$$

where μ is the chemical potential of the electrons, and η is a positive infinitesimal. From the Green's function the independent particle polarizability

$$\chi(\mathbf{r}, \mathbf{r}', t) = -iG_0(\mathbf{r}, \mathbf{r}', t)G_0(\mathbf{r}', \mathbf{r}, -t) \tag{2}$$

and the corresponding screened interaction

$$W(\mathbf{r}, \mathbf{r}', \omega) = v(\mathbf{r}, \mathbf{r}') + v(\mathbf{r}, \mathbf{s})\chi(\mathbf{s}, \mathbf{s}', \omega)W(\mathbf{s}', \mathbf{r}', \omega) \tag{3}$$

can be determined. Here v is the Coulomb kernel, and integration over repeated spatial coordinates ($\mathbf{s}$ and $\mathbf{s}'$) is assumed. Furthermore, the Green's functions and polarizabilities in frequency and time domain are related by a Fourier transformation. The final step is to calculate the interacting Green's function

$$G(\mathbf{r}, \mathbf{r}', \omega) = \frac{1}{\omega - T - V^{\mathrm{H}}(\mathbf{r})\delta(\mathbf{r} - \mathbf{r}') - \Sigma(\mathbf{r}, \mathbf{r}', \omega)} \tag{4}$$

where T is the kinetic energy operator, V^{H} is the Hartree-potential, and $\Sigma(\mathbf{r}, \mathbf{r}', t)$ is the self-energy in the *GW* approximation:

$$\Sigma(\mathbf{r}, \mathbf{r}', t) = iG_0(\mathbf{r}, \mathbf{r}', t)W(\mathbf{r}, \mathbf{r}', t) \tag{5}$$

The poles of the Green's function then determine the QP energies. In principle, this cycle can be continued by evaluating χ in step (2) using the updated Green's function and iterated to self-consistency. It is also possible to obtain partial self-consistency, for instance, by calculating W once and forever using the DFT orbitals and one electron energies and iterating only the Green's function until it is self-consistent [i.e., iterating only eqs 4 and 5].

The most common approximation is, however, the G_0W_0 approximation e.g. used by Hybertsen and Louie.[5] Instead of the poles of the Green's function, this approximation calculates the nodes of the denominator in eq 4

$$E_n^{\mathrm{QP}} = \mathrm{Re}[\langle\phi_n|T + V^H(\mathbf{r}) + \Sigma(E_n^{\mathrm{QP}})|\phi_n\rangle] \tag{6}$$

in the basis of the DFT orbitals. Since this involves only the diagonal elements of the self-energy, solutions of this equation are cheaper to determine than poles of the fully interacting Green's function. Obviously this is a good approximation, if the self-energy is diagonally dominant in the basis of the DFT orbitals. As already pointed out by Hybertsen and Louie this is generally the case, although there is some evidence that iterating the DFT orbitals is important.[6,9,33] This is particularly so for atoms or molecules, since the KS potential and, as a result, the KS orbitals do not decay properly at large distances from the molecule.

The solutions obtained by solving eq 6 are labeled as G_0W_0 in the present work. Furthermore, a commonly used approximation is to linearize the energy dependence in the self-energy in eq 6 at the DFT one-electron energy and determine the nodes of the linearized equation. This yields the following approximate position for the nodes[5,34]

$$E_n^{\mathrm{QP}} - \epsilon_n^{\mathrm{DFT}} = Z_n\mathrm{Re}[\langle\phi_n|T + V^{\mathrm{H}}(\mathbf{r}) + \Sigma(\epsilon_n^{\mathrm{DFT}}) - \epsilon_n^{\mathrm{DFT}}|\phi_n\rangle] \tag{7}$$

where Z_n is related to the derivative of the self-energy at $\epsilon_n^{\mathrm{DFT}}$

$$Z_n = \left(1 - \frac{\partial\mathrm{Re}[\langle\phi_n|\Sigma(\omega)|\phi_n\rangle]}{\partial\omega}\bigg|_{\epsilon_n^{\mathrm{DFT}}}\right)^{-1}$$

The correlation factor Z_n can be also related to the amplitude of the corresponding QP peak and is a measure of the degree of correlation. For the HOMO and LUMO of molecules, Z is commonly between 0.7 and 0.9, corresponding to a low to very low degree of correlation. Solutions of the linearized equations will be labeled as lin-G_0W_0 in the present work, and the first derivative is evaluated using central difference with the step size of $\Delta = \pm 0.1$ eV.

2.2. Technical Details. As in the *GW*100 paper of van Setten et al.,[27] we use the PBE functional for the DFT starting point. However, all calculations include scalar relativistic effects, in contrast to the calculations of van Setten et al. that are based on nonrelativistic potentials. The potentials used in the present work are the *GW* potentials distributed with the latest release of VASP (vasp.5.4), and we followed the recommendations in the VASP manual on which version to use. Generally this means that lower lying semicore states were not correlated in the calculations, except for the alkali and alkali-earth metals, as well

DOI: 10.1021/acs.jctc.6b01150
J. Chem. Theory Comput. 2017, 13, 635−648

as Ti and Ga. For He, we found issues with the originally distributed potential. The `He_GW` potential failed to converge in DFT calculations when the plane wave cutoff was increased, because a ghost state was introduced as the basis set size increased. The potential was slightly modified to remove this problem and will be distributed with the next release. Furthermore, for boron to fluorine the potentials `B_GW_new`, ..., `F_GW_new` were used (also already distributed with vasp.5.4). These potentials include *d* partial waves, whereas the standard *GW* potentials choose the *d* potential as the local potential.

The potentials used in this work are not the most accurate *GW* potentials yet available for VASP. Specifically, we have recently shown that norm-conserving (NC) *GW* potentials are necessary to predict very accurate QP energies for 3*d*, 4*d*, and 5*d* elements[25] with the NC potentials generally increasing the QP binding energies. In our experience, such highly accurate potentials are, however, not required in the present case for the following reasons. For *s* and *p* elements the standard potentials conserve the norm very well to within about 70%, often even 90%. Furthermore, errors introduced by violating the norm-conservation can only occur at very high scattering energies, since the standard *GW*-PAW potentials predict the scattering properties correctly up to about 400 eV. Beyond that energy, the PAW projectors become incomplete. For the elements considered here, we expect that the combination of these two effects means that the results for the HOMO and LUMO will be accurate even though we do not use NC potentials. The only exceptions are copper, neon, fluorine, oxygen, and possibly nitrogen. These elements possess strongly localized 3*d* and 2*p* orbitals. We will return to this point later.

In the calculations presented here we calculate the Green's function, the screened interaction *W* as well as the self-energy in imaginary time and frequency. This has several advantages compared to the full real frequency implementation also available in VASP. The fully frequency dependent version along the real axis requires at least 100, but for molecules with their sharp resonances often even several hundred frequency points to converge. Since the boxes considered in this work are quite large, we also need several thousands of plane waves to describe the frequency dependent screened interaction and Green's function accurately. This becomes very quickly prohibitive. In the imaginary frequency, on the other hand, only relatively few frequency points are required. In the calculations presented here, 16 frequency points and the time and frequency grids discussed by Kaltak et al. are used.[35,36] These 16 points were found to be sufficient to converge the QP energies of the HOMO and LUMO to about 10 meV.[37] The downside of working in the imaginary frequency domain is that the results along the imaginary frequency axis need to be continued to the real axis. This was done using a (16 point) Padé fit following Thiele's reciprocal difference method based on continued fractions.[38] We note that the reported FHI-aims results in ref 27 were— with few problematic exceptions —also obtained using 16 parameter Padé fits. These exceptions are BN, O_3, BeO, MgO, and CuCN where many more points were required. For the other molecules, the 16 parameter Padé fits yielded excellent agreement with Turbomole, which calculates the exact *GW* self-energy along the real axis. Details of our implementation are reported elsewhere.[37]

The other crucial issues are basis set extrapolation and convergence with respect to the box size. To obtain basis set converged results, we used a relatively small box, but one that still faithfully reproduces the character of the HOMO and LUMO. For this box, we performed calculations for the default cutoff as specified by the VASP potentials and calculations for three additional plane wave cutoffs, with the largest calculation corresponding to twice the number of plane waves used in the default setup. These four data points are fitted assuming that the QP energies as a function of the number of plane waves N_{pw} converge like

$$E^{QP}(N_{pw}) = E^{QP}(\infty) + \frac{C}{N_{pw}} \tag{8}$$

where N_{pw} is the number of plane waves in the basis set.[25,39−41] A four point fit and a two point fit with the largest and smallest PW basis set yielded a maximum difference of 10 meV in the QP energies. To illustrate that the basis set dependence is indeed following a $1/N_{pw}$ behavior to great accuracy, we will show data for selected molecules in section 3.2. The only subtlety impeding an accurate and automatic extrapolation is the use of the Padé fit. The slope of the self-energy can vary somewhat between different calculations causing some variations in the predicted QP energies. Extrapolation from these "noisy" data is difficult and error prone. To circumvent this issue, we perform the extrapolation for the self-energy evaluated at the DFT one-electron energies, specifically on $\Delta E = \mathrm{Re}[\langle\phi|T + V^{H} + \Sigma(\epsilon^{DFT})|\phi\rangle] - \epsilon^{DFT}$ instead of $\Delta E = E^{QP} - \epsilon^{DFT}$, and scale the correction by the *Z*-factor at the smallest, i.e. default, PW cutoff. In this way, we neglect variations of the *Z*-factor between different basis sets, but these variations are small and dominated by noise.

A few final comments are in place here. In the calculations presented herein, we calculate *all* orbitals spanned by the PW basis set. This implies that the number of orbitals also increases as the number of plane waves increases. Second, the kinetic energy cutoff for the response function (`ENCUTGW` in VASP) is set to 2/3 of the cutoff used for the plane wave basis of the orbitals (`ENCUT` in VASP). Whenever the PW cutoff for the orbitals is increased, the PW cutoff for the basis set of the response function is increased accordingly. This means that a single parameter, the PW cutoff for the orbitals (`ENCUT`), entirely controls the accuracy of the calculations (at least with respect to the basis sets). Since all the intermediate control parameters are set automatically by VASP, and since the QP energy corrections converge like one over the number of plane waves and orbitals,[25] extrapolation to the infinite basis set limit is straightforward and robust.

Let us now comment on the second point, convergence with respect to the cell size. In plane wave codes, it is common practice to truncate the Coulomb kernel at a certain distance r_c, say half the box size, so that the periodically repeated orbitals can not screen the central atom. The downside of this approach is that it modifies the Coulomb kernel to become[42]

$$\frac{4\pi e^2}{|\mathbf{g}|^2}(1 - \cos(|\mathbf{g}|r_c))$$

where $\mathbf{g}$ is a plane wave vector. Obviously, this modifies the Coulomb kernel at large reciprocal lattice vectors $\mathbf{g}$. In test calculations we found that this spoils the previously mentioned basis set extrapolation (8): as one increases the plane wave cutoff, one moves through maxima and minima of the truncated Coulomb kernel, causing superimposed oscillations in the QP energies. Basis set extrapolation becomes then uncontrolled. To deal with the repeated images, we instead resort to the standard

DOI: 10.1021/acs.jctc.6b01150
J. Chem. Theory Comput. 2017, 13, 635−648

Table 1. Ionization Potential (IP, Negative of HOMO QP Energies) for 100 Molecules Using G_0W_0 and the Linearized lin-G_0W_0 Method[a]

		G_0W_0		lin-G_0W_0		Δ
		GTO[27]	PW	PW	EXP	PW-GTO
1	He	23.49(0.03)	23.38	23.62	*24.59*[46]	−0.11
2	Ne	20.33(0.01)	20.17	20.36	*21.56*[46]	−0.16
3	Ar	15.28(0.03)	15.32	15.42	*15.76*[47]	0.04
4	Kr	13.89(0.16)	13.93	14.03	14.00[48]	0.04
5	Xe	12.02*	12.14	12.22	12.13[49]	0.12*
6	H_2	15.85(0.09)	15.85	16.06	15.43[50]	0.00
7	Li_2	5.05(0.02)	5.09	5.32	4.73[51]	0.04
8	Na_2	4.88(0.03)	4.93	5.06	4.89[52]	0.05
9	Na_4	4.14(0.03)	4.17	4.23	4.27[53]	0.03
10	Na_6	4.34(0.06)	4.34	4.40	4.12[53]	0.00
11	K_2	4.08(0.04)	4.12	4.24	4.06[52]	0.04
12	Rb_2	3.79*	4.02	4.14	3.90[52]	0.23*
13	N_2	15.05(0.04)	14.93	15.06	15.58[54]	−0.12
14	P_2	10.38(0.04)	10.35	10.40	10.62[55]	−0.03
15	As_2	9.67(0.10)	9.59	9.62	10.0[56]	−0.08
16	F_2	15.10(0.04)	14.93	15.08	15.70[57]	−0.17
17	Cl_2	11.31(0.05)	11.32	11.40	*11.49*[58]	0.01
18	Br_2	10.56(0.18)	10.57	10.65	*10.51*[58]	0.01
19	I_2	9.23*	9.52	9.59	*9.36*[59]	0.29*
20	CH_4	14.00(0.06)	14.02	14.14	*13.6*[60]	0.02
21	C_2H_6	12.46(0.06)	12.50	12.58	*11.99*[59]	0.04
22	C_3H_8	11.89(0.06)	11.90	11.98	*11.51*[59]	0.01
23	C_4H_{10}	11.59(0.05)	11.61	11.69	*11.09*[59]	0.02
24	C_2H_4	10.40(0.03)	10.42	10.50	*10.68*[60]	0.02
25	C_2H_2	11.09(0.01)	11.07	11.24	*11.49*[60]	−0.02
26	C_4	10.91(0.03)	10.89	10.97	12.54[61]	−0.02
27	C_3H_6	10.65(0.04)	10.72	10.78	*10.54*[62]	0.07
28	C_6H_6	9.10(0.01)	9.11	9.16	*9.23*[63]	0.01
29	C_8H_8	8.18(0.02)	8.19	8.24	*8.43*[64]	0.01
30	C_5H_6	8.45(0.02)	8.47	8.51	*8.53*[65]	0.02
31	CH_2CHF	10.32(0.02)	10.28	10.36	*10.63*[66]	−0.04
32	CH_2CHCl	9.89(0.02)	9.92	10.00	*10.20*[67]	0.03
33	CH_2CHBr	9.14(0.01)	9.75	9.83	*9.90*[67]	0.61
34	CH_2CHI	9.01*	9.27	9.36	*9.35*[68]	0.26*
35	CF_4	15.60(0.06)	15.41	15.53	*16.20*[69]	−0.19
36	CCl_4	11.21(0.06)	11.20	11.31	*11.69*[59]	−0.01
37	CBr_4	10.22(0.16)	10.25	10.38	*10.54*[70]	0.03
38	CI_4	8.71*	9.11	9.23	*9.10*[71]	0.40*
39	SiH_4	12.40(0.06)	12.40	12.53	*12.3*[72]	0.00
40	GeH_4	12.11(0.04)	12.13	12.24	*11.34*[73]	0.02
41	H_6Si_2	10.41(0.06)	10.44	10.52	*10.53*[74]	0.03
42	$H_{12}Si_5$	9.05(0.05)	9.13	9.19	*9.36*[74]	0.08
43	LiH	6.58(0.04)	6.46	7.20	7.90[75]	−0.12
44	KH	4.99(0.01)	4.97	5.37	8.00[76]	−0.02
45	BH_3	12.96(0.06)	12.95	13.09	12.03[77]	−0.01
46	B_2H_6	11.93(0.06)	11.94	12.04	*11.90*[78]	0.01
47	NH_3	10.39(0.05)	10.32	10.44	*10.82*[79]	−0.07
48	HN_3	10.55(0.02)	10.50	10.56	*10.72*[80]	−0.05
49	PH_3	10.35(0.05)	10.35	10.45	*10.59*[81]	0.00
50	AsH_3	10.21(0.02)	10.26	10.36	*10.58*[82]	0.05
51	H_2S	10.13(0.04)	10.11	10.30	*10.50*[83]	−0.02
52	HF	15.37(0.01)	15.37	15.38	*16.12*[84]	0.00
53	HCl	12.36(0.01)	12.45	12.51	12.79[85]	0.09
54	LiF	10.27(0.03)	10.07	10.45	11.30[86]	−0.20
55	MgF_2	12.50(0.06)	12.41	12.77	13.30[87]	−0.09
56	TiF_4	14.07(0.05)	14.01	14.22	*15.30*[88]	−0.06
57	AlF_3	14.48(0.06)	14.33	14.53	15.45[89]	−0.15
58	BF	10.73(0.05)	10.46	10.67	11.00[90]	−0.27

DOI: 10.1021/acs.jctc.6b01150
J. Chem. Theory Comput. 2017, 13, 635−648

Table 1. continued

		G_0W_0		lin-G_0W_0		Δ
		GTO[27]	PW	PW	EXP	PW-GTO
59	SF_4	12.38(0.07)	12.20	12.29	11.69[91]	−0.18
60	KBr	7.57(0.13)	7.80	8.04	*8.82*[92]	0.23
61	GaCl	9.74(0.07)	9.89	9.99	*10.07*[93]	0.15
62	NaCl	8.43(0.14)	8.47	8.76	*9.80*[92]	0.04
63	$MgCl_2$	11.20(0.07)	11.19	11.41	*11.80*[94]	−0.01
64	AlI_3	9.30*	9.58	9.69	*9.66*[95]	0.28*
65	BN	11.15(0.03)		10.61	11.50	
66	HCN	13.32(0.01)	13.29	13.43	*13.61*[96]	−0.03
67	PN	11.29(0.04)	11.24	11.41	11.88[97]	−0.05
68	N_2H_4	9.37(0.04)	9.33	9.45	*8.98*[98]	−0.04
69	H_2CO	10.46(0.02)	10.42	10.57	10.88[99]	−0.04
70	CH_3OH	10.67(0.05)	10.61	10.72	*10.96*[100]	−0.06
71	CH_3CH_2OH	10.27(0.05)	10.21	10.33	*10.64*[101]	−0.06
72	CH_3CHO	9.66(0.03)	9.63	9.80	*10.24*[102]	−0.03
73	$CH_3CH_2OCH_2CH_3$	9.42(0.05)	9.43	9.52	*9.61*[101]	0.01
74	HCOOH	10.87(0.01)	10.81	10.98	*11.50*[103]	−0.06
75	H_2O_2	11.10(0.01)	10.96	11.12	*11.70*[104]	−0.14
76	H_2O	12.05(0.03)	11.84	12.05	*12.62*[59]	−0.21
77	CO_2	13.46(0.06)	13.36	13.44	*13.77*[105]	−0.10
78	CS_2	9.95(0.05)	9.96	10.01	*10.09*[106]	0.01
79	CSO	11.11(0.05)	11.06	11.13	*11.19*[107]	−0.05
80	COSe	10.43(0.09)	10.42	10.50	10.37[108]	−0.01
81	CO	13.71(0.04)	13.62	13.76	*14.01*[107]	−0.09
82	O_3	11.49(0.03)		12.07	*12.73*[109]	
83	SO_2	12.06(0.06)	11.91	12.04	*12.50*[59]	−0.15
84	BeO	8.60(0.01)		9.50	10.10[110]	
85	MgO	6.75(0.03)		7.10	8.76[111]	
86	$C_6H_5CH_3$	8.73(0.02)	8.75	8.79	*8.82*[63]	0.02
87	C_8H_{10}	8.66(0.02)	8.69	8.73	*8.77*[63]	0.03
88	C_6F_6	9.74(0.07)	9.63	9.69	*10.20*[69]	−0.11
89	C_6H_5OH	8.51(0.01)	8.38	8.43	8.75[112]	−0.13
90	$C_6H_5NH_2$	7.78(0.01)	7.78	7.84	*8.05*[113]	0.00
91	C_5H_5N	9.17(0.01)	9.16	9.31	*9.66*[114]	−0.01
92	guanine	7.87(0.01)	7.85	7.90	*8.24*[115]	−0.02
93	adenine	8.16(0.01)	8.12	8.18	*8.48*[116]	−0.04
94	cytosine	8.44(0.01)	8.40	8.50	*8.94*[115]	−0.04
95	thymine	8.87(0.01)	8.83	8.89	*9.20*[117]	−0.04
96	uracil	9.38(0.01)	9.36	9.55	*9.68*[118]	−0.02
97	NH_2CONH_2	9.46(0.02)	9.35	9.59	*9.80*[83]	−0.11
98	Ag_2	7.08*	7.83	7.95	7.66[119]	0.75*
99	Cu_2	7.78(0.06)	7.19	7.40	7.46[120]	−0.59
100	CuCN	9.56(0.04)		9.99		

[a]For comparison the basis set extrapolated values[27] and the experimental IPs are given (vertical IPs are in italics). If basis set extrapolated values are not specified in ref 27, the AIMS-P16 values are shown in the column GTO (marked by *). The last column shows the differences between GTO and PW results. The * indicates differences to nonbasis set extrapolated values.

trick used in periodic codes: $k \cdot p$ perturbation theory.[43] We calculate the first order change of the orbitals with respect to k[44] and accordingly the head and wings of the polarizability and a correction to the $\mathbf{g} \rightarrow 0$ component of the self-energy. This term corrects the leading monopole−monopole interaction between repeated images but leaves the monopole−dipole and dipole−dipole interactions uncorrected. These two terms fall off like $1/V$ and $1/V^2$, where V is the cell size volume.[45] To deal with this, we perform four calculations at different volumes, with the box size progressively increased by 1 Å and fit the data to

$$a_0 + a_1/V + a_2/V^2 \quad (9)$$

For most molecules the corrections are small and only of the order of 10−20 meV, whereas for the alkali dimers and some polar molecules the corrections can be as large as 100−200 meV. In these cases the correction is very well described by the theoretical equation. We hope to find a better solution in future work, for instance, an explicit subtraction of monopole and dipole interactions between periodic images. In terms of compute time, however, the additional calculations for smaller boxes only require a modest amount of time: since the total compute time scales quadratic to cubic with respect to the number of plane waves, the calculations scale also quadratic to cubic in the volume. Typically we need 12 Å large boxes to obtain results converged to 20 meV with respect to the box

DOI: 10.1021/acs.jctc.6b01150
J. Chem. Theory Comput. 2017, 13, 635−648

size. The additional smaller volumes used for the extrapolation require only half of the compute time of the largest final box.

The final QP energies reported in the next section were obtained by calculating the PBE one-electron HOMO and LUMO for a 25 Å box at an energy cutoff that is 30% increased compared to the VASP default values. The vacuum level, evaluated as the Hartree plus ionic potential, was evaluated at the position furthest from the center of the molecule and subtracted from the PBE one-electron energies. We checked that the DFT one-electron energies are converged to a few meV with this setup. To the DFT one-electron energies, the shift of the QP energies $E^{QP}-\epsilon^{DFT}$ for the largest considered box, box size corrections, and basis set corrections as described above are added. It goes without saying that this procedure is rather involved and since errors are expected to accumulate, we estimate that the present predictions are only accurate to about ±50 meV, where convergence with cell size is the main source of errors and difficult to estimate precisely.

To give a feeling for the required compute time and computational effort, we need to stress that our plane wave code is mainly designed for solids. Nevertheless, a calculation for C_6H_6 in a 10 Å box at the default cutoff takes about 4 h on a single node with 16 Xeon v2 cores. The compute time stays roughly constant if the box size is increased by 1 Å and the number of cores is simultaneously doubled. Furthermore, the compute time is mostly independent of the number of atoms in the box but increases cubically with the box size as the total number of plane waves increases linearly with the box size. By comparison Turbomole, using the def2-TZVP basis and the resolution of the identity method, takes 30 min on a 12 core AMD opteron 6174 for the response and *GW* part of the calculation (the time spent for the DFT part is negligible in comparison).

3. RESULTS

3.1. HOMO for *GW*100. Let us first note on the agreement at the level of DFT (not shown). In general, our values agree exceedingly well with the PBE values reported in the Supporting Information of ref 27. In most cases, our PBE HOMO is located between the basis set extrapolated values and the values obtained with the best basis sets used in the GTO calculations (def2-QZVP). On average, our PW HOMOs agree better with the nonbasis set extrapolated values with a mean deviation (MD) of 7 meV and a mean absolute deviation (MAD) of 19 meV. Compared to the GTO basis set extrapolated values, the MD and MAD are −25 and 30 meV (in both cases, CH_2CHBr was excluded, see below).

van Setten et al.[27] extrapolated the DFT eigenvalues using a cubic polynomial in the inverse of the basis set cardinal number (C_n^{-3}); we believe that this is not appropriate and will overestimate the basis set corrections. It is commonly agreed that DFT calculations converge exponentially with the cardinal number, whereas any correlated wave function calculation converges with the inverse of the basis set size (corresponding roughly to C_n^{-3}).[25−27] This is a result of Kato's cusp condition[121] causing a kink in the many-body wave function as two coordinates approach each other. We have shown that this problem carries over to *GW* calculations.[25] As a one-electron theory, density functional theory does not suffer from this slow convergence. We hence believe that van Setten overestimated the basis set corrections for DFT. This is supported by the observation that our PBE results tend to be closer to the nonextrapolated Gaussian results at the level of def2-QZVP.

We now turn to the QP energies predicted at the level of G_0W_0 shown in Table 1. The agreement between the VASP PW and the GTO results is generally very good. We note that the G_0W_0 approximation used here is identical to the one applied by van Setten et al.[27] Specifically, van Setten determined the nodes of eq 6, and we do exactly the same in the present work. Linearization of the QP eq 7 yields generally somewhat larger QP energies and often improves agreement with experiment slightly (column lin-G_0W_0). This trend has also been observed in a recent benchmark for an unrelated set of molecules.[122] In agreement with van Setten,[27] we have found poles in the self-energy close to the predicted QP energies for BN, O_3, BeO, MgO, and CuCN. Since analytic continuation has difficulties to resolve the precise pole structure of the Green's function, we only report the values obtained from the linearized self-energy.

Our discussion starts with the molecules that show large discrepancies between VASP and GTOs. A large outlier is seemingly CH_2CHBr. However, for this molecule, as well as C_6H_5OH, we found large forces in the preparatory PBE calculations. Double checking the original literature[123] suggests that the *GW*100 paper used incorrect geometries. Since the ultimate purpose is certainly to compare with experiment, we decided to update the geometries to the correct literature values.

Among the remaining molecules, errors are large for compounds containing iodine, rubidium, and silver with a maximum deviation of 400 meV for CI_4 and Rb_2 and 750 meV for Ag_2. However, in ref 27 no basis set extrapolation was performed for these molecules. From CCl_4 to CBr_4, the basis set corrections increase from 300 to 350 meV, suggesting a basis set error of 400 meV for CI_4 using GTOs. Similarly, for Rb_2 the GTO results were not basis set corrected, and estimating the basis set error from Na_2 and K_2 again suggests that the VASP results are accurate. For Ag_2, the difference between VASP and GTO seem on first sight to be too large to be ascribed to basis set errors alone. To resolve the issue, one of us (MvS) repeated the Xe, Rb_2, I_2, CH_2CHI, CI_4, AlI_3, and Ag_2 calculations using scalar relativistic corrections and frozen core SVP, TZVP, and QZVP basis sets. This yielded basis set extrapolated values summarized in Table 2 certainly now in good to very good agreement with the VASP values.

For the remaining molecules, the mean absolute deviation between the two codes and thus two completely different basis sets is only 60 meV, if we also exclude Cu_2. For Cu_2, the

Table 2. IP (Negative HOMO G_0W_0 QP Energies) and G_0W_0 LUMO for Selected Molecules[a]

		IP		LUMO	
		GTO	PW	GTO	PW
5	Xe	12.22	12.14	−0.07	0.28
12	Rb_2	4.07	4.02	−0.85	−0.74
19	I_2	9.48	9.52	−2.28	−2.21
34	CH_2CHI	9.13	9.27	0.56	0.37
38	CI_4	8.97	9.11	−2.47	−2.42
64	AlI_3	9.50	9.58	−1.18	−1.02
98	Ag_2	7.96	7.83	−1.40	−1.35

[a]The GTO values have been calculated using frozen core potentials and scalar relativistic corrections and are extrapolated to the infinite basis set limit.

DOI: 10.1021/acs.jctc.6b01150
J. Chem. Theory Comput. 2017, 13, 635−648

fluorine containing compounds, H_2O, as well as Ne the ionization potentials (IPs) are smaller in VASP, which we will now show to be related to slight deficiencies in the PAW potentials. Copper, neon, and fluorine and, to a lesser extent, oxygen are particularly difficult to describe using a plane wave based approach, since the 3*d* and 2*p* electrons are strongly localized. To cope with this, the Cu, F, and Ne potentials are already the three smallest core and hardest potentials used in the present work; but still, the partial waves do not conserve the norm exactly, which results in errors, if an electron is scattered into a plane wave with very high kinetic energy.[25] To determine this error, we performed calculations with norm-conserving (or almost norm-conserving) *GW* potentials for the molecules Cu_2, N_2, F_2, CF_4, HF, BF, SF_4, and H_2O reported in Table 3 using

Table 3. IP (Negative HOMO G_0W_0 QP Energies) for Selected Molecules Calculated for a 9 Å Box for the Standard *GW* Potentials and Normconserving *GW* Potentials[a]

		GW PAW	NC *GW* PAW	Δ
13	N_2	14.98	15.02	−0.04
16	F_2	14.97	15.13	−0.15
35	CF_4	15.42	15.58	−0.16
52	HF	15.39	15.32	0.06
58	BF	10.42	10.46	−0.04
59	SF_4	12.19	12.26	−0.07
76	H_2O	11.86	11.94	−0.09
99	Cu_2	7.03	7.53	−0.50

[a]Results differ from the previous table, since calculations in Table 1 have been performed for larger boxes and include a correction for the box size error. The column Δ reports the difference between the standard PAW and NC PAW potential.

the potentials `Cu_sv_GW_nc`, `N_h_GW`,...,`F_h_GW`. Except for HF, the QP energies are clearly shifted toward higher binding energies in these calculations, and the discrepancies to the GTO calculations are reduced to an acceptable level of 100 meV. We also note that the PAW error increases from nitrogen, over oxygen to fluorine. HF and BF are exceptions, since the HOMOs possess predominantly hydrogen and boron character and, therefore, do not depend strongly on the F potential (we note that the HF results were already accurate using the standard potentials). Finally, the standard carbon and boron potentials used here are already almost norm conserving, and hence negligible changes are found for carbon based compounds with harder potentials (not shown).

The final case worthwhile mentioning is KBr. Here the *GW*100 paper[27] reports relatively large extrapolation errors of 130 meV, indicating that in this case the GTO based extrapolation might be inaccurate.

For the remaining systems, we find the agreement to be excellent. Specifically, for all considered organic molecules the absolute differences are typically below 50 meV, with very few outliers. This clearly demonstrates that plane wave codes can be competitive in terms of precision with GTOs. Certainly the agreement between GTOs and PWs is better than originally reported in the *GW*100 paper, a point discussed in more detail in the next section.

3.2. Basis Set Convergence and Comparison to Other PW Calculations. In Figure 1, we show the convergence of the HOMO with respect to the plane wave cutoff for the orbitals. This cutoff also determines the total number of orbitals as well as the cutoff for the response function. The number of plane

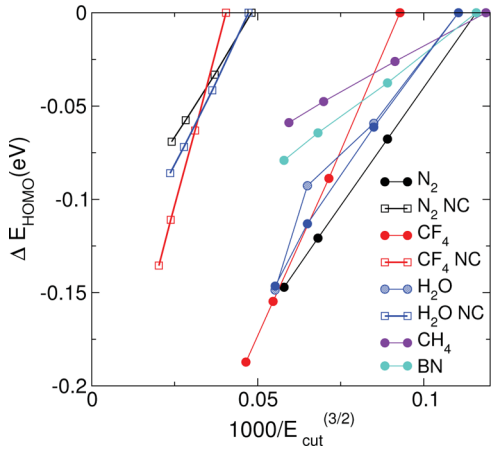

Figure 1. Convergence of QP HOMO with respect to the employed cutoff for various materials. For N_2, CF_4, and H_2O, results are shown for two potentials, the standard *GW* potentials, as well as NC potentials. The slopes are steeper for the NC potentials, which is particularly obvious for CF_4. For H_2O results for two box sizes (8 and 9 Å) are shown (see text).

waves and total orbitals is proportional to one over the cutoff to the power of 3/2. It is clearly visible that the curves follow almost exactly a straight line. In a few cases, outliers are visible. For instance for H_2O, we have included results for two box sizes 8 and 9 Å. The 9 Å box results have a slight jump, which is not present for the 8 Å box. However, this outlier is small (about 10 meV) and changes extrapolated results only by less than 10 meV. Usually the outliers could be dealt with by just changing the box size slightly. We believe that they are related to "shell"-effects, i.e. a sudden increase in the number of plane waves when the cutoff is changed through certain values. Furthermore, the analytic continuation is not always entirely well behaved and can cause changes of the order of 20 meV. Overall, the plot demonstrates that extrapolation with respect to the energy-cutoff is very well under control and can be done with great accuracy.

As noted before, the differences between the GTO and the Berkeley *GW* calculations reported in ref 27 are more sizable. If we exclude the difficult multipole cases, BN, O_3, MgO, and BeO, the mean absolute deviation between Berkeley *GW* and basis set extrapolated GTOs was 0.2 eV in ref 27, whereas it is reduced to 0.05 eV for VASP PAW potentials (for the same subset). We speculate that this is mostly related to neglecting basis set extrapolation errors or — less likely — to an inaccurate treatment of the core−valence interaction. Typically our basis set corrections are of the order of 300−400 meV at the default cutoff and therefore very sizable. Even doubling the number of basis functions and therefore increasing the compute time by a factor of about 8 (cubic scaling) reduces the error only by a factor 2, to about 150−200 meV. Hence, calculations without basis set corrections are hardly affordable or practicable, and it is certainly advisible to perform an extrapolation whenever possible.

For the core−valence interaction, we emphasize that VASP always evaluates the interaction at the level of Hartree−Fock if correlated calculations are performed. More precisely, VASP calculates the PBE core orbitals on the fly and then recalculates the action of the PBE core states on the valence states using the Hartree−Fock approximation. Not doing so can have a sizable effect on the QP energies for heavier atoms.[34] We are not aware

DOI: 10.1021/acs.jctc.6b01150
J. Chem. Theory Comput. 2017, 13, 635−648

Table 4. LUMO QP Energies for Selected Molecules Using G_0W_0 and the Linearized lin-G_0W_0[a]

		G_0W_0			lin-G_0W_0		Δ
		AIMS-P16	GTO-EXTRA	PW	PW	EXP	PW-GTO
5	Xe	4.28		0.70	0.70		−3.58[+]
7	Li_2	−0.63	−0.75(0.04)	−0.61	−0.54		0.14
8	Na_2	−0.55	−0.66(0.70)	−0.60	−0.56	−0.54	0.06
9	Na_4	−1.01	−1.15(0.90)	−1.07	−1.03	−0.91[124]	0.08
10	Na_6	−0.97	−1.13(0.10)	−1.07	−1.03		0.06
11	K_2	−0.65	−0.75(0.05)	−0.74	−0.70	−0.50	0.01
12	Rb_2	−0.62		−0.74	−0.70	−0.50[124]	−0.12*
14	P_2	−0.72	−1.08(0.08)	−0.99	−0.97	−0.68[125]	0.09
15	As_2	−0.85	−1.52(0.35)	−1.07	−1.06	−0.74[126]	0.45
16	F_2	−0.70	−1.23(0.14)	−0.96	−0.84	*−1.24*[127]	0.27
17	Cl_2	−0.89	−1.40(0.12)	−1.25	−1.22	*−1.02*[127]	0.15
18	Br_2	−1.40	−1.96(0.29)	−1.99	−1.97	*−1.60*[127]	−0.03
19	I_2	−1.68		−2.21	−2.20	*−1.70*[127]	−0.53*
20	CH_4	2.45	2.03(0.35)	0.63	0.63		−1.40[+]
26	C_4	−2.94	−3.15(0.06)	−3.09	−3.08	−3.88[128]	0.06
29	C_8H_8	0.06	−0.12(0.02)	−0.05	−0.02	−0.57[129]	0.07
32	CH_2CHCl	1.42	1.17(0.03)	1.19	1.25		0.02[+]
36	CCl_4	−0.01	−0.54(0.13)	−0.32	−0.28		0.22
37	CBr_4	−1.08	−1.56(0.29)	−1.47	−1.44		0.09
38	CI_4	−2.14	–	−2.42	−2.40		−0.28*
42	$H_{12}Si_5$	0.16	0.00(0.07)	0.03	0.05		0.03
43	LiH	−0.07	−0.16(0.09)	−0.07	−0.04	−0.34[130]	0.09
44	KH	−0.18	−0.32(0.01)	−0.25	−0.22		0.07
45	BH_3	0.12	0.03(0.05)	0.03	0.08	−0.04[131]	0.00
54	LiF	0.09	−0.01(0.01)	0.17	0.17		0.18
55	MgF_2	−0.14	−0.31(0.06)	−0.29	−0.28		0.02
56	TiF_4	−0.60	−1.06(0.13)	−0.79	−0.66	−2.50[132]	0.27
57	AlF_3	0.16	−0.23(0.10)	0.08	0.09		0.31
59	SF_4	0.38	−0.10(0.13)	0.07	0.12	−1.50[133]	0.17
60	KBr	−0.31	−0.42(0.06)	−0.32	−0.31	−0.64[134]	0.10
61	GaCl	−0.02	−0.39(0.15)	−0.19	−0.15		0.20
62	NaCl	−0.39	−0.42(0.01)	−0.46	−0.43	−0.73[134]	−0.04
63	$MgCl_2$	−0.43	−0.68(0.08)	−0.61	−0.59		0.07
64	AlI_3	−0.80		−1.02	−0.99		−0.22*
72	CH_3CHO	1.05	0.83(0.05)	0.87	0.87		0.04[+]
74	HCOOH	1.91	1.59(0.00)	1.64	1.72		0.05[+]
76	H_2O	2.37	2.01(0.16)	1.04	1.04		−0.97[+]
78	CS_2	−0.20	−0.55(0.09)	−0.42	−0.40	−0.55[135]	0.13
82	O_3	−2.30	−2.69(0.11)	−2.50	−2.52	−2.10[136]	0.19
83	SO_2	−1.00	−1.49(0.12)	−1.25	−1.19	−1.11[137]	0.24
84	BeO	−2.56	−2.72(0.04)	−2.73	−2.37		−0.01
85	MgO	−1.89	−2.13(0.09)	−2.05	−2.12		0.08
88	C_6F_6	0.66	0.36(0.08)	0.24	0.27	−0.70[138]	−0.12[+]
94	cytosine	0.26	0.01(0.01)	0.12	0.15	−0.23[139]	0.11
95	thymine	0.06	−0.18(0.01)	−0.06	−0.04	*0.29*[140]	0.12
96	uracil	0.01	−0.25(0.01)	−0.11	−0.09	*0.22*[140]	0.14
98	Ag_2	−1.05		−1.35	−1.31	*−1.10*[141]	−0.30*
99	Cu_2	−0.92	−1.23(0.08)	−1.24	−1.21	−0.84[142]	−0.01
100	CuCN	−1.65	−1.85(0.05)	−1.91	−1.81	*−1.47*[143]	−0.06

[a]For comparison, the nonbasis set extrapolated values (AIMS-P16), the basis set extrapolated values,[27] and the negative of the experimental electron affinities are shown (vertical attachment energies are in italics). Differences between PW and GTO are shown in the last column. The [+] indicates energies above the vacuum level, and * indicates differences to nonbasis set extrapolated values.

of other pseudopotential codes following a similar route. This might be responsible for a small part of the errors in the reported Berkeley *GW* calculations of ref 27, if heavier atoms are involved.

Calculations for another fairly large set of molecules have been reported by Govoni and Galli using the West code.[24] Twenty-nine molecules are identical to the *GW*100 set considered here. The mean absolute difference between the basis set extrapolated GTO results and the VASP results for this subset is 60 meV, whereas the difference between the West results and the basis set extrapolated GTO results is about twice as large 120 meV (mean absolute difference between VASP and

DOI: 10.1021/acs.jctc.6b01150
J. Chem. Theory Comput. 2017, 13, 635−648

West is 90 meV). In many cases, the West IPs are too small indicating again basis set incompleteness errors. Anyhow, the West results are closer to the basis set converged values than the *GW* Berkeley results.

3.3. Comparison to Experiment. When comparing the present results against the experimental ionization energies, a mean absolute error of 0.5 eV is observed. This large discrepancy is not unexpected given that in this computational approach self-consistency, vertex corrections, and finite temperature effects are omitted. However, we can comment on the biggest outliers in the set. A first example is C_4: it is well-known that the smaller C_2 molecule is particularly challenging to describe, owing to strong electron correlation.[144] For the larger cluster we expect similar effects, hence the inclusion of the vertex should improve the agreement with the experiment. We have a similar expectation for the case of F_2. Our conjecture is substantiated by previous electron propagator calculations,[145] where the poles of the Green's function in the Lehmann representation were located to give the IP, and where a comparable mismatch to experiment was ascribed to the poor description of dynamic correlation. For AlF_3, LiF, and KH we have to bear in mind that the experimental value for a vertical transition was not available; therefore, geometry relaxations may explain the mismatch. This is only partially true for KH, where the inclusion of adiabatic effects in the perturbative calculations still leaves a sizable disagreement (~2 eV);[146] in this case it is not completely unreasonable to call for a further assessment of the experimental value.

3.4. Linearized QP-HOMO for *GW*100. We now turn to results obtained by first linearizing the self-energy and then determining the QP energy from this linearized equation. This procedure is in our experience more "robust" and better behaved than seeking the poles in the nonlinearized equation. The main issue of the latter approach is that, in the G_0W_0 approximation, the first pole in the self-energy is approximately located at the energy of the DFT HOMO minus the first excitation energy in the DFT (LUMO-HOMO):

$$\epsilon_{\mathrm{HOMO}} - (\epsilon_{\mathrm{LUMO}} - \epsilon_{\mathrm{HOMO}})$$

This is a simple Auger like excitation, where the hole has sufficient energy, i.e. is sufficiently below the HOMO to be able to excite an electron−hole pair. As discussed by van Setten, such poles lead to multiple solutions for the QP energy[27] and make the determination of the QP energies difficult for molecules with small excitation energies. These poles are, however, an artifact of the G_0W_0 approximation. If the *GW* procedure were done self-consistently, the first pole in the self-energy would move to approximately

$$E^{\mathrm{QP}}_{\mathrm{HOMO}} - (E^{\mathrm{QP}}_{\mathrm{LUMO}} - E^{\mathrm{QP}}_{\mathrm{HOMO}})$$

In other words, at the valence band edge (HOMO) and conduction band edge (LUMO) the self-energy never possesses poles. However, in a single shot procedure and when starting from much too small band gaps, the quasiparticle energy E^{QP} might move into regions where the self-energy evaluated from DFT orbitals has a pole. Linearization at the DFT eigenenergies resolves this issue, as the G_0W_0 self-energy has no poles in the direct vicinity of the DFT HOMO. The problem is also less severe, if the calculations are done self-consistently or when starting from a prescription that yields larger HOMO−LUMO Kohn−Sham gaps, as shown in a recent evaluation of the difference between the quasi-particle orbital energies and their linearized counterparts by Govoni et al.[24] Therein it is shown that, for a wide range of molecules, this difference is substantially more pronounced for *GW* calculations on a PBE reference state than if a hybrid functional with nonlocal exchange is used.

In summary, we feel that for code benchmarking as well as for a comparison with experiment determining the poles of the linearized equation is preferable, at least, if a PBE reference state is employed. However, it also needs to be emphasized that for comparison with the already published *GW*100 data, it is of paramount importance to follow exactly the procedures laid out in the initial *GW*100 paper.

3.5. LUMO for *GW*100. The calculated LUMOs are shown in Table 4. A few important comments are in place here. First, the table reports the QP energy of the lowest unoccupied orbital in the preceding DFT calculations to maintain compatibility with the previous publication. In some cases (Xe, H_2O, CH_2CHCl, CH_3CHO, and HCOOH) PW calculations predict at the DFT level a very weakly bound LUMO+1 state (just below the vacuum level) whose G_0W_0 QP energy is below the QP state corresponding to the DFT LUMO level. These energy levels are not shown in Table 4.

If we consider the G_0W_0 values corresponding to the DFT LUMOs, the agreement between the *GW*100 reference GTO data and plane waves is reasonable, although not quite as good as for the HOMO. Specifically troublesome is the observation that the GTO calculations sometimes predict too positive LUMOs. Admittedly, box size convergence can be troublesome for QP energies above the vacuum level, and we therefore only show a few selected positive LUMOs — those where we are confident that convergence to 50 meV was attained for the cell sizes considered in our calculations. All positive (unbound) G_0W_0 LUMOs are marked by a superscript "+" sign in the last column. The differences are particularly striking for Xe, H_2O, and CH_4.

To investigate this issue, we compared the DFT-LUMOs of the PW and GTO calculations (the latter are available upon request to MvS) and found that the deviations between PWs and GTOs are much larger than for the DFT HOMOs on average, and especially large for the problematic cases, i.e. the largest outliers in the subsequent QP calculations.

For the other cases with larger discrepancies, we now show that the previously chosen GTO basis sets were often not sufficiently flexible to describe unoccupied orbitals. This is supported by several observations. (i) Basis set corrections using GTOs are much larger for the LUMO than for the HOMO, as for instance exemplified for As_2, F_2, or Cl_2. To make this very clear, we have included in Table 4 both the basis set extrapolated values (with estimated error bars), as well as the values at the largest considered GTO basis set. (ii) Nonbasis set extrapolated GTO values deviate markedly from PW results. As before, these are marked by a star superscript in the last column. GTO basis set extrapolated values are tabulated in Table 2 and clearly improve the agreement with the PW results. For Xe, where the discrepancy was previously 3.6 eV, the error is reduced to about 0.3 eV. Furthermore, we recalculated the QP energies of H_2O and CH_4 using Dunning correlation consistent basis sets and found basis set extrapolated G_0W_0 QP energies of 1.00 and 0.89 eV, now in excellent and reasonable agreement with the PW results. All in all, we therefore conclude that the Gaussian basis set results for unoccupied states need to be considered with some caution, and Dunning correlation

DOI: 10.1021/acs.jctc.6b01150
J. Chem. Theory Comput. 2017, 13, 635−648

consistent basis sets are seemingly better suited to predict accurate values.

If we restrict the comparison between PWs and GTOs to states below the vacuum level, we find the agreement to be generally, as for the HOMO, rather satisfactory. Differences are about a factor two larger than for the HUMO, but considering the previous discussion on the possible issues with the Gaussian basis sets for unoccupied orbitals, this is certainly not astonishing.

Finally, concerning the agreement with the experiment, we find a similar absolute deviation as for the first ionization energies (compare with Table 1). To make the comparison between the LUMO energies and the experiment more immediate, the second last column reports the negative of the experimental electron affinities. LUMO energies are overall in quite satisfactory agreement with experiment.

4. DISCUSSIONS AND CONCLUSIONS

The main purpose of the present work is a careful comparison of *GW* QP energies obtained using Gaussian type orbitals and plane waves. One important motivation was that the values reported for the Berkeley *GW* code were typically 200 meV smaller than the basis set extrapolated GTO results. However, the Gaussian basis set extrapolation also often increased the predicted QP energies by some 100 meV. Since basis set extrapolation using GTOs is not necessarily accurate, and since the Berkeley *GW* calculations are often closer to the uncorrected values than the basis set extrapolated values, we felt that it is important to bring in a third independent set of calculations, hopefully confirming one or the other of the previous values.

The main outcome of our work is that our VASP predicted HOMOs are in excellent agreement with the basis set extrapolated GTO results. We believe this establishes beyond doubt that the values reported in ref 27 are very reliable and can be used as a rigorous benchmark for future implementations. In the few cases (iodine compounds, Br_2 and Ag_2), where the GTO calculations were not extrapolated to the basis set limit, we find — not unexpectedly — that the nonbasis set extrapolated GTO values underestimate the IP by about 300−400 meV. The present work also reports basis set extrapolated GTO values for these molecules finding good agreement with VASP PW results.

Although the mean absolute deviation between our PAW PW results and the GTO results is only 60 meV, we found larger discrepancies for molecules containing copper, fluorine, and nitrogen. We traced these differences back to the use of non-normconserving PAW potentials: using normconserving PAW potentials the agreement between PW calculations and GTOs improves further.

For the LUMO, results are slightly less satisfactory. Agreement between GTOs and PWs is good for QP energies below the vacuum level, although even for those there are more outliers and the average deviation is larger. For instance, differences are sizable for some seemingly simple dimers. We attribute this to very large basis set corrections for GTOs for some molecules (e.g., 700 meV for As_2).

If the predicted QP LUMOs are above the vacuum level, the differences between the PW and GTO results can be sizable. Our explanation for this behavior is that the GTO basis sets employed in ref 27 are not always sufficiently flexible to model unoccupied states. This is particularly true for atoms and small dimers, where the LUMO has a character that is very different from a linear combination of atomic like orbitals. In most cases, these basis set issues lead to small but noticeable errors on the level of DFT, but they are dramatically amplified at the level of G_0W_0. For Xe, H_2O, and CH_4, GTO calculations with improved basis sets have been reported here finding very good to good agreement with the PW results.

If we disregard the slightly disconcerting propagation of errors in going from DFT to G_0W_0 for LUMOs, we are satisfied by the agreement between plane waves and Gaussian type orbitals. As already stated, for the HOMO the mean absolute deviation is only 60 meV, which is excellent if one considers that the computational details are so different. Furthermore, our results have been obtained using the *GW* PAW potentials distributed with vasp.5.4, so that similar calculations, e.g. for molecules adsorbed on surfaces, can be readily performed using the projector augmented wave method.

AUTHOR INFORMATION

Corresponding Author

*E-mail: georg.kresse@univie.ac.at.

Notes

The authors declare no competing financial interest.

ACKNOWLEDGMENTS

This work was supported by the Austrian Science Fund (FWF) within the *Spezialforschungsbereich Vienna Computational Materials Laboratory* (SFB ViCoM, F41) and the *Deutsche Forschungsgruppe Research Unit* FOR 1346. P.L. is grateful to the China Scholarship Council (CSC)-FWF Scholarship Program. Computational resources were provided by the Vienna Scientific Cluster (VSC) and supercomputing facilities of the Université catholique de Louvain (CISM/UCL).

REFERENCES

(1) Hedin, L. New Method for Calculating the One-Particle Green's Function with Application to the Electron-Gas Problem. *Phys. Rev.* **1965**, *139*, A796−A823.

(2) Hanke, W.; Sham, L. J. Many-Particle Effects in the Optical Excitations of a Semiconductor. *Phys. Rev. Lett.* **1979**, *43*, 387−390.

(3) Strinati, G.; Mattausch, H. J.; Hanke, W. Dynamical Correlation Effects on the Quasiparticle Bloch States of a Covalent Crystal. *Phys. Rev. Lett.* **1980**, *45*, 290−294.

(4) Strinati, G.; Mattausch, H. J.; Hanke, W. Dynamical aspects of correlation corrections in a covalent crystal. *Phys. Rev. B: Condens. Matter Mater. Phys.* **1982**, *25*, 2867−2888.

(5) Hybertsen, M. S.; Louie, S. G. Electron correlation in semiconductors and insulators: Band gaps and quasiparticle energies. *Phys. Rev. B: Condens. Matter Mater. Phys.* **1986**, *34*, 5390−5413.

(6) van Schilfgaarde, M.; Kotani, T.; Faleev, S. Quasiparticle Self-Consistent *GW* Theory. *Phys. Rev. Lett.* **2006**, *96*, 226402.

(7) Shishkin, M.; Kresse, G. Self-consistent *GW* calculations for semiconductors and insulators. *Phys. Rev. B: Condens. Matter Mater. Phys.* **2007**, *75*, 235102.

(8) Fuchs, F.; Furthmüller, J.; Bechstedt, F.; Shishkin, M.; Kresse, G. Quasiparticle band structure based on a generalized Kohn-Sham scheme. *Phys. Rev. B: Condens. Matter Mater. Phys.* **2007**, *76*, 115109.

(9) Faleev, S. V.; van Schilfgaarde, M.; Kotani, T. All-Electron Self-Consistent *GW* Approximation: Application to Si, MnO, and NiO. *Phys. Rev. Lett.* **2004**, *93*, 126406.

(10) Caruso, F.; Rinke, P.; Ren, X.; Scheffler, M.; Rubio, A. Unified description of ground and excited states of finite systems: The self-consistent GW approach. *Phys. Rev. B: Condens. Matter Mater. Phys.* **2012**, *86*, 081102.

DOI: 10.1021/acs.jctc.6b01150
J. Chem. Theory Comput. 2017, 13, 635−648

(11) Caruso, F.; Rinke, P.; Ren, X.; Rubio, A.; Scheffler, M. Self-consistent GW: All-electron implementation with localized basis functions. *Phys. Rev. B: Condens. Matter Mater. Phys.* **2013**, *88*, 075105.
(12) Kaplan, F.; Weigend, F.; Evers, F.; van Setten, M. J. Off-Diagonal Self-Energy Terms and Partially Self-Consistency in GW Calculations for Single Molecules: Efficient Implementation and Quantitative Effects on Ionization Potentials. *J. Chem. Theory Comput.* **2015**, *11*, 5152−5160.
(13) Kaplan, F.; Harding, M. E.; Seiler, C.; Weigend, F.; Evers, F.; van Setten, M. J. Quasi-Particle Self-Consistent GW for Molecules. *J. Chem. Theory Comput.* **2016**, *12*, 2528−2541.
(14) Lischner, J.; Sharifzadeh, S.; Deslippe, J. R.; Neaton, J. B.; Louie, S. G. Effects of self-consistency and plasmon-pole models on GW calculations for closed-shell molecules. *Phys. Rev. B: Condens. Matter Mater. Phys.* **2014**, *90*, 115130.
(15) Koval, P.; Foerster, D.; Sánchez-Portal, D. Fully self-consistent GW and quasiparticle self-consistent GW for molecules. *Phys. Rev. B: Condens. Matter Mater. Phys.* **2014**, *89*, 155417.
(16) Ren, X.; Rinke, P.; Blum, V.; Wieferink, J.; Tkatchenko, A.; Sanfilippo, A.; Reuter, K.; Scheffler, M. Resolution-of-identity approach to Hartree-Fock, hybrid density functionals, RPA, MP2 and GW with numeric atom-centered orbital basis functions. *New J. Phys.* **2012**, *14*, 053020.
(17) Blase, X.; Attaccalite, C.; Olevano, V. First-principles *GW* calculations for fullerenes, porphyrins, phtalocyanine, and other molecules of interest for organic photovoltaic applications. *Phys. Rev. B: Condens. Matter Mater. Phys.* **2011**, *83*, 115103.
(18) Bruneval, F. Ionization energy of atoms obtained from GW self-energy or from random phase approximation total energies. *J. Chem. Phys.* **2012**, *136*, 194107.
(19) van Setten, M. J.; Weigend, F.; Evers, F. *J. Chem. Theory Comput.* **2013**, *9*, 232−246.
(20) Wilhelm, J.; Del Ben, M.; Hutter, J. GW in the Gaussian and Plane Waves Scheme with Application to Linear Acenes. *J. Chem. Theory Comput.* **2016**, *12*, 3623−3635.
(21) Foerster, D.; Koval, P.; Sánchez-Portal, D. An O(N3) implementation of Hedin's GW approximation for molecules. *J. Chem. Phys.* **2011**, *135*, 074105.
(22) Ke, S. H. All-electron GW methods implemented in molecular orbital space: Ionization energy and electron affinity of conjugated molecules. *Phys. Rev. B: Condens. Matter Mater. Phys.* **2011**, *84*, 205415.
(23) Laflamme Janssen, J.; Rousseau, B.; Cote, M. Efficient dielectric matrix calculations using the Lanczos algorithm for fast many-body G0W0 implementations. *Phys. Rev. B: Condens. Matter Mater. Phys.* **2015**, *91*, 125120.
(24) Govoni, M.; Galli, G. Large Scale GW Calculations. *J. Chem. Theory Comput.* **2015**, *11*, 2680−2696.
(25) Klimeš, J.; Kaltak, M.; Kresse, G. Predictive GW calculations using plane waves and pseudopotentials. *Phys. Rev. B: Condens. Matter Mater. Phys.* **2014**, *90*, 075125.
(26) Bruneval, F.; Marques, M. A. L. Benchmarking the Starting Points of the GW Approximation for Molecules. *J. Chem. Theory Comput.* **2013**, *9*, 324−329.
(27) van Setten, M. J.; Caruso, F.; Sharifzadeh, S.; Ren, X.; Scheffler, M.; Liu, F.; Lischner, J.; Lin, L.; Deslippe, J. R.; Louie, S. G.; Yang, C.; Weigend, F.; Neaton, J. B.; Evers, F.; Rinke, P. GW100: Benchmarking G_0W_0 for Molecular Systems. *J. Chem. Theory Comput.* **2015**, *11*, 5665−5687. PMID: 26642984.
(28) Deslippe, J.; Samsonidze, G.; Strubbe, D. a.; Jain, M.; Cohen, M. L.; Louie, S. G. BerkeleyGW: A massively parallel computer package for the calculation of the quasiparticle and optical properties of materials and nanostructures. *Comput. Phys. Commun.* **2012**, *183*, 1269−1289.
(29) Schindlmayr, A. Analytic evaluation of the electronic self-energy in the GW approximation for two electrons on a sphere. *Phys. Rev. B: Condens. Matter Mater. Phys.* **2013**, *87*, 075104.
(30) Shih, B.-C.; Xue, Y.; Zhang, P.; Cohen, M. L.; Louie, S. G. Quasiparticle Band Gap of ZnO: High Accuracy from the Conventional G^0W^0 Approach. *Phys. Rev. Lett.* **2010**, *105*, 146401.
(31) Friedrich, C.; Müller, M. C.; Blügel, S. Band convergence and linearization error correction of all-electron *GW* calculations: The extreme case of zinc oxide. *Phys. Rev. B: Condens. Matter Mater. Phys.* **2011**, *83*, 081101;Erratum: **2011**, *84*, 039906E.
(32) Bruneval, F.; Gonze, X. Accurate GW self-energies in a plane-wave basis using only a few empty states: Towards large systems. *Phys. Rev. B: Condens. Matter Mater. Phys.* **2008**, *78*, 085125.
(33) Bruneval, F.; Vast, N.; Reining, L. Effect of self-consistency on quasiparticles in solids. *Phys. Rev. B: Condens. Matter Mater. Phys.* **2006**, *74*, 045102.
(34) Shishkin, M.; Kresse, G. Implementation and performance of the frequency-dependent GW method within the PAW framework. *Phys. Rev. B: Condens. Matter Mater. Phys.* **2006**, *74*, 035101.
(35) Kaltak, M.; Klimeš, J.; Kresse, G. Low Scaling Algorithms for the Random Phase Approximation: Imaginary Time and Laplace Transformations. *J. Chem. Theory Comput.* **2014**, *10*, 2498−2507.
(36) Kaltak, M.; Klimeš, J.; Kresse, G. Cubic scaling algorithm for the random phase approximation: Self-interstitials and vacancies in Si. *Phys. Rev. B: Condens. Matter Mater. Phys.* **2014**, *90*, 054115.
(37) Liu, P.; Kaltak, M.; Klimeš, J.; Kresse, G. Cubic scaling GW: Towards fast quasiparticle calculations. *Phys. Rev. B: Condens. Matter Mater. Phys.* **2016**, *94*, 165109.
(38) Baker, G. A. J. *Essentials of Padé Approximants*; Academic Press: New York, 1975; Chapter 18.
(39) Harl, J.; Kresse, G. Cohesive energy curves for noble gas solids calculated by adiabatic connection fluctuation-dissipation theory. *Phys. Rev. B: Condens. Matter Mater. Phys.* **2008**, *77*, 045136.
(40) Shepherd, J. J.; Grüneis, A.; Booth, G. H.; Kresse, G.; Alavi, A. Convergence of many-body wave-function expansions using a plane-wave basis: From homogeneous electron gas to solid state systems. *Phys. Rev. B: Condens. Matter Mater. Phys.* **2012**, *86*, 035111.
(41) Björkman, T.; Gulans, A.; Krasheninnikov, A. V.; Nieminen, R. M. van der Waals Bonding in Layered Compounds from Advanced Density-Functional First-Principles Calculations. *Phys. Rev. Lett.* **2012**, *108*, 235502.
(42) Rozzi, C. A.; Varsano, D.; Marini, A.; Gross, E. K. U.; Rubio, A. Exact Coulomb cutoff technique for supercell calculations. *Phys. Rev. B: Condens. Matter Mater. Phys.* **2006**, *73*, 205119.
(43) Baldereschi, A.; Tosatti, E. Mean-value point and dielectric properties of semiconductors and insulators. *Phys. Rev. B: Condens. Matter Mater. Phys.* **1978**, *17*, 4710−4717.
(44) Gajdoš, M.; Hummer, K.; Kresse, G.; Furthmüller, J.; Bechstedt, F. Linear optical properties in the projector-augmented wave methodology. *Phys. Rev. B: Condens. Matter Mater. Phys.* **2006**, *73*, 045112.
(45) Makov, G.; Payne, M. Periodic boundary conditions in ab initio calculations. *Phys. Rev. B: Condens. Matter Mater. Phys.* **1995**, *51*, 4014−4022.
(46) Kelly, R. L. Atomic and Ionic Spectrum Lines below 2000 Angstroms: Hydrogen through Krypton *J. Phys. Chem. Ref. Data* **1987**, *16*, Supplement 1.
(47) Weitzel, K.-M.; Mähnert, J.; Penno, M. ZEKE-PEPICO investigations of dissociation energies in ionic reactions. *Chem. Phys. Lett.* **1994**, *224*, 371−380.
(48) Wetzel, R. C.; Baiocchi, F. A.; Hayes, T. R.; Freund, R. S. Absolute cross sections for electron-impact ionization of the rare-gas atoms by the fast-neutral-beam method. *Phys. Rev. A: At., Mol., Opt. Phys.* **1987**, *35*, 559−577.
(49) Schäfer, H.; Rabeneck, H. Massenspektroskopische Untersuchung der Borfluorid-Komplexe ABF4. *Z. Anorg. Allg. Chem.* **1987**, *545*, 224−226.
(50) McCormack, E.; Gilligan, J. M.; Cornaggia, C.; Eyler, E. E. Measurement of high Rydberg states and the ionization potential of H_2. *Phys. Rev. A: At., Mol., Opt. Phys.* **1989**, *39*, 2260−2263.
(51) Dugourd, P.; Rayane, D.; Labastie, P.; Vezin, B.; Chevaleyre, J.; Broyer, M. Measurements of lithium cluster ionization potentials. *Chem. Phys. Lett.* **1992**, *197*, 433−437.

DOI: 10.1021/acs.jctc.6b01150
J. Chem. Theory Comput. 2017, 13, 635−648

(52) Kappes, M. M.; Radi, P.; Schär, M.; Schumacher, E. Photoionization measurements on dialkali monohalides generated in supersonic nozzle beams. *Chem. Phys. Lett.* **1985**, *113*, 243−248.
(53) Herrmann, A.; Leutwyler, S.; Schumacher, E.; Wöste, L. On Metal-Atom Clusters IV. Photoionization thresholds and multiphoton ionization spectra of alkali-metal molecules. *Helv. Chim. Acta* **1978**, *61*, 453−487.
(54) Trickl, T.; Cromwell, E. F.; Lee, Y. T.; Kung, A. H. Stateselective ionization of nitrogen in the X $2\Sigma_g^+$ v_+=0 and v_+=1 states by twocolor (1+ 1) photon excitation near threshold. *J. Chem. Phys.* **1989**, *91*, 6006−6012.
(55) Bulgin, D. K.; Dyke, J. M.; Morris, A. HeI photoelectron spectrum of the $P_2(X^1\ \Sigma_g^+)$ molecule. *J. Chem. Soc., Faraday Trans. 2* **1976**, *72*, 2225−2232.
(56) Lau, K. H.; Brittain, R. D.; Hildenbrand, D. L. Vaporization of arsenic trisulfide and the dissociation energy of arsenic monosulfide. *J. Phys. Chem.* **1982**, *86*, 4429−4432.
(57) Van Lonkhuyzen, H.; De Lange, C. A. High-resolution UV photoelectron spectroscopy of diatomic halogens. *Chem. Phys.* **1984**, *89*, 313−322.
(58) Dyke, J. M.; Josland, G. D.; Snijders, J. G.; Boerrigter, P. M. Ionization energies of the diatomic halogens and interhalogens studied with relativistic hartree-fock-slater calculations. *Chem. Phys.* **1984**, *91*, 419−424.
(59) Kimura, K.; Katsumata, S.; Achiba, Y.; Yamazaki, T.; Iwata, S. *Handb. HeI Photoelectron Spectra Fundam. Org. Compd.*; Japan Scientific Soc. Press: Tokyo, 1981.
(60) Bieri, G.; Åsbrink, L. 30.4-nm He(II) photoelectron spectra of organic molecules. *J. Electron Spectrosc. Relat. Phenom.* **1980**, *20*, 149−167.
(61) Ramanathan, R.; Zimmerman, J. A.; Eyler, J. R. Ionization potentials of small carbon clusters. *J. Chem. Phys.* **1993**, *98*, 7838−7845.
(62) Plemenkov, V.; Villem, Y.; Villem, N.; Bolesov, I.; Surmina, L.; Yakushkina, N.; Formanovskii, A. Photoelectron spectra of polyalkylcyclopropenes and polyalkylcyclopropanes. *Zh. Obs. Khim.* **1981**, *51*, 2076.
(63) Howell, J. O.; Goncalves, J. M.; Amatore, C.; Klasinc, L.; Wightman, R. M.; Kochi, J. K. Electron transfer from aromatic hydrocarbons and their π-complexes with metals. Comparison of the standard oxidation potentials and vertical ionization potentials. *J. Am. Chem. Soc.* **1984**, *106*, 3968−3976.
(64) Fu, E. W.; Dunbar, R. C. Photodissociation spectroscopy and structural rearrangements in ions of cyclooctatetraene, styrene, and related molecules. *J. Am. Chem. Soc.* **1978**, *100*, 2283−2288.
(65) Kiselev, V.; Sakhabutdinov, A.; Shakirov, I.; Zverev, V.; Konovalov, A. Bis reactants in Diels-Alder reactions. VII. Preparation and properties of polyadducts of reactions of bis-(polymethylcyclopentadienes) and bis(maleimides). *Zh. Org. Khim.* **1992**, *28*, 2244.
(66) Bieri, G.; von Niessen, W.; Åsbrink, L.; Svensson, A. The He(II) photoelectron spectra of the fluorosubstituted ethylenes and their analysis by the Green's function method. *Chem. Phys.* **1981**, *60*, 61−79.
(67) Cambi, R.; Ciullo, G.; Sgamellotti, A.; Tarantelli, F.; Fantoni, R.; Giardini-guidoni, A.; McCarthy, I. E.; di Martino, V. An (e, 2e) spectroscopic invistigation and a green's function study of the ionization of chloro- and bromo-ethylene. *Chem. Phys. Lett.* **1983**, *101*, 477−484.
(68) Wittel, K.; Bock, H.; Manne, R. Photoelectron spectra of iodo ethylenes. *Tetrahedron* **1974**, *30*, 651−658.
(69) Bieri, G.; Åsbrink, L.; Von Niessen, W. V. 30.4-nm He(II) Photoelectron spectra of organic molecules: Part IV. Fluoro-compounds (C, H, F). *J. Electron Spectrosc. Relat. Phenom.* **1981**, *23*, 281−322.
(70) Dixon, R. N.; Murrell, J. N.; Narayan, B. The photoelectron spectra of the halomethanes. *Mol. Phys.* **1971**, *20*, 611−623.
(71) Jonkers, G.; Lange, C.; Snijders, J. G. Effects of relativity in the He(I) Photoelecron Spectrum of CI4. *Chem. Phys.* **1982**, *69*, 109−114.
(72) Roberge, R.; Sandorfy, C.; Matthews, J. I.; Strausz, O. P. The far ultraviolet and HeI photoelectron spectra of alkyl and fluorine substituted silane derivatives. *J. Chem. Phys.* **1978**, *69*, 5105−5112.
(73) Potts, A. W.; Price, W. C. The Photoelectron Spectra of Methane, Silane, Germane and Stannane. *Proc. R. Soc. London, Ser. A* **1972**, *326*, 165−179.
(74) Bock, H.; Ensslin, W.; Feher, F.; Freund, R. Photoelectron spectra and molecular properties. LI. Ionization potentials of silanes Si_nH_{2n+2}. *J. Am. Chem. Soc.* **1976**, *98*, 668−674.
(75) NIST Chemistry WebBook. 2015. http://webbook.nist.gov/chemistry/ (accessed Jan 16, 2017).
(76) Farber, M.; Srivastava, R. D.; Moyer, J. W. Mass-spectrometric determination of the thermodynamics of potassium hydroxide and minor potassiumcontaining species required in magnetohydrodynamic power systems. *J. Chem. Thermodyn.* **1982**, *14*, 1103−1113.
(77) Ruscic, B.; Mayhew, C. A.; Berkowitz, J. Photoionization studies of $(BH_3)_n$ (n = 1,2). *J. Chem. Phys.* **1988**, *88*, 5580−5593.
(78) Åsbrink, L.; Svensson, A.; von Niessen, W.; Bieri, G. 30.4-nm He(II) photoelectron spectra of organic molecules: Part V. Hetero-compounds containing first-row elements (C, H, B, N, O, F). *J. Electron Spectrosc. Relat. Phenom.* **1981**, *24*, 293−314.
(79) Baumgaertel, H.; Jochims, H. W.; Ruehl, E.; Bock, H.; Dammel, R.; Minkwitz, J.; Nass, R. Photoelectron spectra and molecular properties. 112. Photoelectron and photoionization mass spectra of the fluoroamines NH_3-nFn. *Inorg. Chem.* **1989**, *28*, 943−949.
(80) Cvitaš, T.; Klasinc, L. High resolution photoelectron spectrum of hydrazoic acid. *J. Chem. Soc., Faraday Trans. 2* **1976**, *72*, 1240−1244.
(81) Cowley, A. H.; Kemp, R. A.; Lattman, M.; McKee, M. L. Lewis base behavior of methylated and fluorinated phosphines. Photoelectron spectroscopic investigation. *Inorg. Chem.* **1982**, *21*, 85−88.
(82) Demuth, R. Photoelektronenspektren von einigen Trihalogensilylphosphanen und -arsanen X_3SiER_2 (X = F, Cl; E = N, P, As; R = H, CH_3)/Photoelectron Spectra of Some Trihalogensilyl Phosphines and Arsines X_3SiER_2 (X = F, Cl; E = N, P, As; R = H, CH_3). *Zeitschrift für Naturforsch. B* **1977**, *32*, 1252.
(83) Bieri, G.; Åsbrink, L.; von Niessen, W. 30.4-nm He (II) photoelectron spectra of organic molecules: Part VII. Miscellaneous compounds. *J. Electron Spectrosc. Relat. Phenom.* **1982**, *27*, 129−178.
(84) Banna, M. S.; Shirley, D. A. Molecular photoelectron spectroscopy at 132.3 eV. The second-row hydrides. *J. Chem. Phys.* **1975**, *63*, 4759−4766.
(85) Wang, R.; Dillon, M. A.; Spence, D. Electron spectroscopy of hydrogen chloride from 5 to 19 eV. *J. Chem. Phys.* **1984**, *80*, 63−69.
(86) Berkowitz, J.; Tasman, H. A.; Chupka, W. A. Double-Oven Experiments with Lithium Halide Vapors. *J. Chem. Phys.* **1962**, *36*, 2170−2179.
(87) Hildenbrand, D. L. Mass-Spectrometric Studies of Bonding in the Group IIA Fluorides. *J. Chem. Phys.* **1968**, *48*, 3657−3665.
(88) Dyke, J. M.; Haggerston, D.; Wright, A.; Morris, A.; van Lenthe, E.; Snijders, J. A study of the transition metal tetrafluorides (TiF_4, ZrF_4, HfF_4) using high temperature ultraviolet photoelectron spectroscopy. *J. Electron Spectrosc. Relat. Phenom.* **1997**, *85*, 23−33.
(89) Dyke, J. M.; Kirby, C.; Morris, A.; Gravenor, B.; Klein, R.; Rosmus, P. A study of aluminium monofluoride and aluminium trifluoride by high-temperature photoelectron spectroscopy. *Chem. Phys.* **1984**, *88*, 289−298.
(90) Farber, M.; Srivastava, R. D. Electron and thermal dissociation of BF_3(g). *J. Chem. Phys.* **1984**, *81*, 241−244.
(91) Fisher, E. R.; Kickel, B. L.; Armentrout, P. Collision-induced dissociation and charge transfer reactions of SF_x^+ (x = 1−5): Thermochemistry of sulfur fluoride ions and neutrals. *J. Chem. Phys.* **1992**, *97*, 4859−4870.
(92) Potts, A. W.; Price, W. C. Photoelectron Studies of Ionic Materials using Molecular Beam Techniques. *Phys. Scr.* **1977**, *16*, 191−196.
(93) Grabandt, O.; Mooyman, R.; De Lange, C. He(I) Photoelectron spectroscopy of the gallium monohalides. *Chem. Phys.* **1990**, *143*, 227−238.

DOI: 10.1021/acs.jctc.6b01150
J. Chem. Theory Comput. 2017, 13, 635−648

(94) Lee, E. P. F.; Potts, A. W. An Investigation of the Valence Shell Electronic Structure of Alkaline Earth Halides by Using ab initio s.c.f. Calculations and Photoelectron Spectroscopy. *Proc. R. Soc. London, Ser. A* **1979**, *365*, 395−411.
(95) Barker, G. K.; Lappert, M. F.; Pedley, J. B.; Sharp, G. J.; Westwood, N. P. C. Bonding studies of boron and the Group 3−5 elements. Part XV. He(I) photoelectron spectra of monomeric Group 3 trihalide, trimethyl, and mixed halogenomethyl species. *J. Chem. Soc., Dalton Trans.* **1975**, *18*, 1765−1771.
(96) Kreile, J.; Schweig, A.; Theil, W. Experimental and theoretical investigation of the photoionization of hydrogen cyanide. *Chem. Phys. Lett.* **1982**, *87*, 473−476.
(97) Bulgin, D. K.; Dyke, J. M.; Morris, A. Vacuum ultraviolet photoelectron spectrum of the PN(X 1 Σ+) molecule. *J. Chem. Soc., Faraday Trans. 2* **1977**, *73*, 983−990.
(98) Vovna, V.; Vilesov, F.; Lopatin, S. Photoelectron spectra of hydrazine and some alkyl derivatives. *Opt. Spectrosc.* **1975**, *38*, 143−144.
(99) Ohno, K.; Okamura, K.; Yamakado, H.; Hoshino, S.; Takami, T.; Yamauchi, M. Penning Ionization of HCHO, CH_2CH_2, and CH_2CHCHO by Collision with He(23S) Metastable Atoms. *J. Phys. Chem.* **1995**, *99*, 14247−14253.
(100) Vorob'ev, A. S.; Furlei, I. I.; Sultanov, A. S.; Khvostenko, V. I.; Leplyanin, G. V.; Derzhinskii, A. R.; Tolstikov, G. A. Mass spectrometry of resonance capture of electrons and photo-electron spectroscopy of molecules of ethylene oxide, ethylene sulfide, and their derivatives. *Bull. Acad. Sci. USSR, Div. Chem. Sci.* **1989**, *38*, 1388−1394.
(101) Ohno, K.; Imai, K.; Harada, Y. Variations in reactivity of lone-pair electrons due to intramolecular hydrogen bonding as observed by Penning ionization electron spectroscopy. *J. Am. Chem. Soc.* **1985**, *107*, 8078−8082.
(102) Johnson, K.; Powis, I.; Danby, C. A photoelectronphotoion coincidence study of acetaldehyde and ethylene oxide molecular ions. *Chem. Phys.* **1982**, *70*, 329−343.
(103) von Niessen, W.; Bieri, G.; Åsbrink, L. 30.4-nm He (II) photoelectron spectra of organic molecules. *J. Electron Spectrosc. Relat. Phenom.* **1980**, *21*, 175−191.
(104) Ashmore, F. S.; Burgess, A. R. Study of some medium size alcohols and hydroperoxides by photoelectron spectroscopy. *J. Chem. Soc., Faraday Trans. 2* **1977**, *73*, 1247−1261.
(105) Eland, J. H. D.; Berkowitz, J. Photoionization mass spectrometry of HI and DI at high resolution. *J. Chem. Phys.* **1977**, *67*, 5034−5039.
(106) Schweig, A.; Thiel, W. Photoionization cross sections: He I- and He II-photoelectron spectra of homologous oxygen and sulphur compounds. *Mol. Phys.* **1974**, *27*, 265−268.
(107) Potts, A.; Williams, T. The observation of forbidden transitions in He II photoelectron spectra. *J. Electron Spectrosc. Relat. Phenom.* **1974**, *3*, 3−17.
(108) Cradock, S.; Duncan, W. Photoelectron spectra of OCSe and SCSe. *J. Chem. Soc., Faraday Trans. 2* **1975**, *71*, 1262−1268.
(109) Katsumata, S.; Shiromaru, H.; Kimura, T. Photoelectron Angular Distribution and Assignment of Photoelectron Spectrum of Ozone. *Bull. Chem. Soc. Jpn.* **1984**, *57*, 1784−1788.
(110) Theard, L. P.; Hildenbrand, D. L. Heat of Formation of $Be_2O(g)$ by Mass Spectrometry. *J. Chem. Phys.* **1964**, *41*, 3416−3420.
(111) Dalleska, N.; Armentrout, P. Guided ion beam studies of reactions of alkaline earth ions with O2. *Int. J. Mass Spectrom. Ion Processes* **1994**, *134*, 203−212.
(112) Ballard, R.; Jones, J.; Read, D.; Inchley, A.; Cranmer, M. He(I) photoelectron studies of liquids and gases. *Chem. Phys. Lett.* **1987**, *137*, 125−129.
(113) Furin, G.; Sultanov, A.; Furlei, I. I. Photoelectronic spectra of fluorine-containing aromatic amines. *Bull. Acad. Sci. USSR, Div. Chem. Sci.* **1987**, *36*, 530−534.
(114) Kobayashi, T.; Nagakura, S. Photoelectron spectra of aminopyridines and cyanopyridines. *J. Electron Spectrosc. Relat. Phenom.* **1974**, *4*, 207−212.
(115) Hush, N.; Cheung, A. S. Ionization potentials and donor properties of nucleic acid bases and related compounds. *Chem. Phys. Lett.* **1975**, *34*, 11−13.
(116) Lin, J.; Yu, C.; Peng, S.; Akiyama, I.; Li, K.; Lee, L. K.; LeBreton, P. R. Ultraviolet photoelectron studies of the ground-state electronic structure and gas-phase tautomerism of purine and adenine. *J. Am. Chem. Soc.* **1980**, *102*, 4627−4631.
(117) Dougherty, D.; Wittel, K.; Meeks, J.; McGlynn, S. P. Photoelectron spectroscopy of carbonyls. Ureas, uracils, and thymine. *J. Am. Chem. Soc.* **1976**, *98*, 3815−3820.
(118) Palmer, M. H.; Simpson, I.; Platenkamp, R. J. The electronic structure of flavin derivatives. *J. Mol. Struct.* **1980**, *66*, 243−263.
(119) Beutel, V.; Krämer, H.-G.; Bhale, G. L.; Kuhn, M.; Weyers, K.; Demtroder, W. High-resolution isotope selective laser spectroscopy of Ag_2 molecules. *J. Chem. Phys.* **1993**, *98*, 2699−2708.
(120) Franzreb, K.; Wucher, A.; Oechsner, H. Electron impact ionization of small silver and copper clusters. *Z. Phys. D: At., Mol. Clusters* **1990**, *17*, 51−56.
(121) Kato, T. On the eigenfunctions of many-particle systems in quantum mechanics. *Comm. Pure Appl. Math.* **1957**, *10*, 151−177.
(122) Scherpelz, P.; Govoni, M.; Hamada, I.; Galli, G. Implementation and Validation of Fully Relativistic GW Calculations: SpinOrbit Coupling in Molecules, Nanocrystals, and Solids. *J. Chem. Theory Comput.* **2016**, *12*, 3523−3544.
(123) Weast, R. C.; Astle, M. J. *CRC Handbook of Chemistry and Physics*; 92nd ed.; CRC Press; New York, 2011.
(124) McHugh, K. M.; Eaton, J. G.; Lee, G. H.; Sarkas, H. W.; Kidder, L. H.; Snodgrass, J. T.; Manaa, M. R.; Bowen, K. H. Photoelectron spectra of the alkali metal cluster anions: $Na^-_{n=25}$, $K^-_{n=27}$, $Rb^-_{n=23}$, and $Cs^-_{n=23}$. *J. Chem. Phys.* **1989**, *91*, 3792−3793.
(125) Jones, R. O.; Ganteför, G.; Hunsicker, S.; Pieperhoff, P. Structure and spectroscopy of phosphorus cluster anions: Theory (simulated annealing) and experiment (photoelectron detachment). *J. Chem. Phys.* **1995**, *103*, 9549−9562.
(126) Lippa, T. P.; Xu, S.-J.; Lyapustina, S. A.; Nilles, J. M.; Bowen, K. H. Photoelectron spectroscopy of As^-,As_2^-,As_3^-,As_4^-, and As_5^-. *J. Chem. Phys.* **1998**, *109*, 10727−10731.
(127) Ayala, J. A.; Wentworth, W. E.; Chen, E. C. M. Electron attachment to halogens. *J. Phys. Chem.* **1981**, *85*, 768−777.
(128) Arnold, D. W.; Bradforth, S. E.; Kitsopoulos, T. N.; Neumark, D. M. Vibrationally resolved spectra of C_2-C_{11} by anion photoelectron spectroscopy. *J. Chem. Phys.* **1991**, *95*, 8753−8764.
(129) Miller, T. M.; Viggiano, A. A.; Miller, A. E. S. Electron Attachment and Detachment: Cyclooctatetraene. *J. Phys. Chem. A* **2002**, *106*, 10200−10204.
(130) Sarkas, H. W.; Hendricks, J. H.; Arnold, S. T.; Bowen, K. H. Photoelectron spectroscopy of lithium hydride anion. *J. Chem. Phys.* **1994**, *100*, 1884−1888.
(131) Wickham-Jones, C. T.; Moran, S.; Ellison, G. B. Photoelectron spectroscopy of BH_3^-. *J. Chem. Phys.* **1989**, *90*, 795−806.
(132) Boltalina, O.; Borshchevskii, A.; Sidorov, L.; Chepurnykh, V. Enthalpy of the Formation of TiF_5^- Anion in a Gas Phase. *Zh. Fiz. Khim. SSSR* **1991**, *65*, 488−491.
(133) Stevens Miller, A. E.; Miller, T. M.; Viggiano, A. A.; Morris, R. A.; Van Doren, J. M.; Arnold, S. T.; Paulson, J. F. Negative ion chemistry of SF_4. *J. Chem. Phys.* **1995**, *102*, 8865−8873.
(134) Miller, T. M.; Leopold, D. G.; Murray, K. K.; Lineberger, W. C. Electron affinities of the alkali halides and the structure of their negative ions. *J. Chem. Phys.* **1986**, *85*, 2368−2375.
(135) Cavanagh, S. J.; Gibson, S. T.; Lewis, B. R. High-resolution photoelectron spectroscopy of linear ← bent polyatomic photodetachment transitions: The electron affinity of CS_2. *J. Chem. Phys.* **2012**, *137*, 144304.
(136) Arnold, D. W.; Xu, C.; Kim, E. H.; Neumark, D. M. Study of low-lying electronic states of ozone by anion photoelectron spectroscopy of O_3^-. *J. Chem. Phys.* **1994**, *101*, 912−922.
(137) Nimlos, M. R.; Ellison, G. B. Photoelectron spectroscopy of sulfur-containing anions (SO_2^-, S_3^-, and S_2O^-). *J. Phys. Chem.* **1986**, *90*, 2574−2580.

DOI: 10.1021/acs.jctc.6b01150
J. Chem. Theory Comput. 2017, 13, 635−648

(138) Eustis, S. N.; Wang, D.; Bowen, K. H.; Naresh Patwari, G. Photoelectron spectroscopy of hydrated hexafluorobenzene anions. *J. Chem. Phys.* **2007**, *127*, 114312.
(139) Schiedt, J.; Weinkauf, R.; Neumark, D. M.; Schlag, E. Anion spectroscopy of uracil, thymine and the amino-oxo and amino-hydroxy tautomers of cytosine and their water clusters. *Chem. Phys.* **1998**, *239*, 511−524.
(140) Aflatooni, K.; Gallup, G. A.; Burrow, P. D. Electron Attachment Energies of the DNA Bases. *J. Phys. Chem. A* **1998**, *102*, 6205−6207.
(141) Handschuh, H.; Cha, C.; Bechthold, P. S.; Gantefor, G.; Eberhardt, W. Electronic shells or molecular orbitals: Photoelectron spectra of Ag_n^- clusters. *J. Chem. Phys.* **1995**, *102*, 6406−6422.
(142) Taylor, K. J.; Pettiette-Hall, C. L.; Cheshnovsky, O.; Smalley, R. E. Ultraviolet photoelectron spectra of coinage metal clusters. *J. Chem. Phys.* **1992**, *96*, 3319−3329.
(143) Wu, X.; Qin, Z.; Xie, H.; Cong, R.; Wu, X.; Tang, Z.; Fan, H. Photoelectron Imaging and Theoretical Studies of Group 11 Cyanides MCN (M = Cu, Ag, Au). *J. Phys. Chem. A* **2010**, *114*, 12839−12844.
(144) Curtiss, L. A.; Redfern, P. C.; Raghavachari, K. Gaussian-4 theory. *J. Chem. Phys.* **2007**, *126*, 084108.
(145) Golab, J. T.; Thies, B. S.; Yeager, D. L.; Nichols, J. a. The ionization potentials of F_2:A comparison of multiconfigurational electron propagator (MCEP) with other large scale methods using the same basis set. *J. Chem. Phys.* **1986**, *84*, 284−299.
(146) Rayne, S.; Forest, K. Survey of main group compounds (HBr) at the Gaussian-4 level of theory: Adiabatic ionization energies and enthalpies of formation. *Comput. Theor. Chem.* **2011**, *974*, 163−179.

DOI: 10.1021/acs.jctc.6b01150
J. Chem. Theory Comput. 2017, 13, 635−648